Journal of Catalysis **197,** 160–171 (2001)
doi:10.1006/jcat.2000.3066, available online at http://www.idealibrary.com on IDEAL®

MCM-48-Supported Vanadium Oxide Catalysts, Prepared by the Molecular Designed Dispersion of $VO(acac)_2$: A Detailed Study of the Highly Reactive MCM-48 Surface and the Structure and Activity of the Deposited VO_x

M. Baltes,*,[1] K. Cassiers,* P. Van Der Voort,* B. M. Weckhuysen,† R. A. Schoonheydt,† and E. F. Vansant*

*Laboratory of Adsorption and Catalysis, Department of Chemistry, University of Antwerpen (U.I.A.), Universiteitsplein 1, 2610 Wilrijk, Belgium; and †Centrum voor Oppervlaktechemie en Katalyse, Departement Interfasechemie, K. U. Leuven, Kardinaal Mercierlaan 92, 3001 Heverlee, Belgium

Received June 23, 2000; revised September 15, 2000; accepted September 15, 2000

The molecular designed dispersion of vanadyl acetylacetonate ($VO(acac)_2$) is used to prepare MCM-48-supported vanadium oxide catalysts. The complex is deposited on the MCM-48 surface and subsequently thermally converted into the supported vanadium oxide. A thorough study of the interaction of the $VO(acac)_2$ with the MCM-48 support by ESR spectroscopy and chemical methods reveals that the MCM-48 surface exhibits a remarkably higher chemical reactivity in comparison to amorphous silica, which is attributed to the presence of very reactive strained siloxane bridges on the MCM-48 surface. According to the BET, XRD, and FTIR study of the supported vanadium oxide catalysts the unique structural properties of MCM-48 are maintained. Characterization by FTIR, Raman, and UV–vis diffuse reflectance spectroscopy reveals the presence of different VO_x structures (monomers, polymers, and crystals) as a function of the vanadium loading (0–6.5 wt% V). The oxidation of methanol similarly shows increasing conversion and formaldehyde yields with increasing loading. Structural characterization of the catalyst after the reaction reveals that the MCM-48-supported vanadium oxides withstand catalytic reaction conditions.

Key Words: **MCM-48; supported vanadium oxide; $VO(acac)_2$.**

INTRODUCTION

Mesoporous molecular sieves of the M41S family, first described in 1992 (1, 2), have very promising properties for potential use as selective adsorbant, molecular sieve, or catalytic support. These materials exhibit surface areas exceeding 1000 m^2/g and a very narrow pore size distribution in the mesoporous range (typically 2–10 nm). The MCM-41 type materials with a hexagonal structure have received widespread interest, whereas the cubic MCM-48 has not received much attention because of the poorly reproducible synthesis. However, the introduction of the so-called gemini surfactants, with general formula $[C_nH_{2n+1}N^+(CH_3)_2-(CH_2)_s-N^+(CH_3)_2C_mH_{2m+1}]\cdot 2Br^-$ (abbreviated *gemini n-s-m*), was a major breakthrough in the development of a reproducible synthesis of high-quality MCM-48 (3, 4). MCM-48 materials can be prepared with high crystallinity features, surface areas around 1500 m^2/g, and very narrow pore size distributions ($d_p = 2$–4 nm). By an appropriate choice of the gemini surfactant (chain and spacer lengths) and the synthesis conditions, it is possible to tune the pore size of the MCM-48 material (4).

Despite the great potential use, until now attention has been drawn to the synthesis and there have only been a few reports on the surface properties and the modification of this material. An important step in the activation of the MCM-48 substrates for use in catalytic applications, is the modification with catalytically active transition metals or transition metal oxides. A novel synthesis method of grafting transition metal oxides on high-surface-area supports is the molecular designed dispersion (MDD) technique (5–10). This method consists of two steps: in a first step, a neutral transition metal acetylacetonate complex (e.g., in this study $VO(acac)_2$) is anchored to the surface of an oxide support. In general, the complex can interact with the support in two distinct ways: (1) by hydrogen bonding between the acac ligand and the surface hydroxyls and (2) by ligand exchange with formation of a covalent metal–oxygen–support bonding and loss of a ligand as acetylacetone (Hacac). In a second step, the adsorbed complex is thermally converted in an oxygen-containing atmosphere, yielding a highly uniform and dispersed supported transition metal oxide catalyst. The molecular designed dispersion can be carried out both in a liquid phase (by stirring the support in the dissolved complex at room temperature) or a gas phase modification process (by sublimation of the complex in vacuum and subsequent reaction with the support). The MDD technique has been studied in detail using silica and alumina as supports (8, 9). The reaction mechanism

[1] To whom correspondence should be addressed. Fax: +32-3-820.23.74. E-mail: baltes@uia.ua.ac.be.

0021-9517/01 $35.00

and the preparation of the final supported oxide catalyst depends on the support properties, the geometry of the complex and the synthesis procedure.

In this paper we will discuss the postsynthesis modification of MCM-48, by the designed deposition of $VO(acac)_2$. The interaction of the complex with the MCM-48 surface is compared with an amorphous silica support. After thermal conversion of the adsorbed complexes, FTIR, Raman, and UV–vis diffuse reflectance spectroscopy are used to elucidate the structure of the supported VO_x phase. The oxidation of methanol is used as a chemical probe reaction to determine the catalytic properties and the structural stability of the MCM-48 supported VO_x catalysts.

METHODS

The MCM-48 support in this study was prepared using the 16–12–16 gemini surfactant, with the formula $[C_{16}H_{33}\text{-}N^+(CH_3)_2\text{-}(CH_2)_{12}\text{-}N^+(CH_3)_2\text{-}C_{16}H_{33}]\cdot 2Br^-$. This surfactant is prepared by refluxing 1,12-dibromodocane and *N,N*-dimethylhexadecylamine in acetone for 24 h, followed by a recrystallization from acetone. To synthesize the MCM-48, the surfactant is dissolved in water. To obtain basic pH conditions, NaOH is added. After a few minutes TEOS ($Si(OC_2H_5)_4$) is added. The molar gel composition is ($GEM/NaOH/H_2O/TEOS = 0.06/0.6/150/1$). The solution is stirred for 2 h at room temperature. Subsequently, the entire solution is put in an autoclave at 100°C for 5 days. After filtration, the resulting white solid is returned to the autoclave with 20 g fresh water per gram of product, and placed at 100°C for an additional 4 days. The final product is obtained by calcination of the precursor in ambient air (heating rate 2°C/min to 550°C).

Silica gel (Kieselgel 60, Merck) was thermally pretreated in air for 17 h at 700°C. The specific surface area of the silica (S_{BET}) was 340 m^2/g. The surface modification reaction with HMDS (1,1,1,3,3,3-hexamethyldisilazane) is performed in fully methylated glassware (three neck bottle and reflux condenser). The HMDS is allowed to reflux during 30 min, before the silica or MCM-48 samples are introduced. Subsequently, the HMDS reaction is carried out for 5 h.

The deposition of the $VO(acac)_2$ complex is carried out in a liquid phase reaction at room temperature. The support was stirred for 1 h in a solution of the $VO(acac)_2$ complex in zeolite dried toluene. The reaction vessel was purged with a stream of dry nitrogen. After the reaction the modified support was filtered, washed with fresh solvent, and dried under vacuum. One washing cycle consists of washing 1 g of the reacted substrate with an aliquot of 25 mL of solvent, before drying.

The samples obtained after modification were stored in a nitrogen glove box to avoid hydration until analysis was completed and subsequently calcined to form the supported vanadium oxide catalysts. Calcination was performed in a programmable oven (25–500°C; heating rate 2°C/min; isothermal period 17 h) in air.

In order to determine the amount of vanadium on the support, the samples were first stirred in hot sulfuric acid (2.5 mol L^{-1}) for 15 min. After filtration, H_2O_2 is added and the vanadium concentration is measured colorimetrically at 450 nm (11).

X-Ray diffraction patterns were collected on a Philips PW1840 powder diffractometer (45 kV, 30 mA), using Ni-filtered Cu$K\alpha$ radiation. Porosity and surface area studies were performed on a Quantachrome Autosorb-1-MP automated gas adsorption system. Pore size distributions in the mesoporous region were calculated using the density functional theory (12). Photoacoustic infrared spectra were recorded on a Nicolet 20 SX spectrometer, equipped with a McClelland Photoacoustic cell. Thermogravimetric measurements were performed with a Mettler TG50 thermobalance, equipped with a M3 microbalance and connected to a TC10A processor. UV–vis diffuse reflectance spectra were obtained at room temperature with a Varian Cary 5 UV–vis–NIR spectrometer equipped with an integration sphere. The spectra were recorded against a halon white reflectance standard. ESR spectra were taken with a Bruker ESP300E spectrometer in X-band (9.5 GHz) with a double rectangular TE_{104} mode cavity at room temperature and at 120 K. The modulation frequency and amplitude were 100 kHz and 5 G, respectively. The ESR spectra were simulated with the QPOW program of the University of Illinois at Urbana–Champaign. FT-Raman spectra were recorded on a Nicolet Nexus FT-Raman spectrometer with a Ge detector. All samples were measured at room temperature in a 180° reflective sampling configuration, with a 1064-nm Nd-YAG excitation laser.

The oxidation of methanol was carried out in a fixed-bed continuous flow reactor at 400°C and atmospheric pressure. Prior to the reaction 0.2 g catalyst was treated by flowing a He/O_2 mixture at 400°C for 16 h (overnight), in order to remove physisorbed water. An 80 mL/min He/O_2/MeOH (88/8/4 mol%) flow was used as reactant mixture. Reaction products were analyzed by gas chromatography on a 2 m × 1/8″ Porapak T column (Alltech Inc.). The catalytic activity and selectivity were measured at the steady state, which was reached after 1 h time-on-stream.

RESULTS AND DISCUSSION

The Synthesis of MCM-48-Supported Vanadium Oxide by the Designed Deposition of $VO(acac)_2$

Physical characterization. The synthesis of pure silica MCM-48 has already been studied and discussed in detail in previous publications (4, 6). The optimized synthesis process using the 16–12–16 gemini surfactant enables the creation of MCM-48 with surface areas in the range 1200–1600 m^2/g and pore volumes exceeding 1.2 mL/g. The

TABLE 1

XRD and BET Characteristics of the Synthesized MCM-48-Supported Vanadium Oxides in Comparison to the Blank MCM-48 Support

	V (mmol/g)	V/nm^2	S_{BET} (m^2/g)	r_p (nm)	V_p (mL/g)	a (nm)
Blank MCM-48	0	0	1275	1.63	1.15	7.92
VO_x/MCM-48	0.2	0.1	1189	1.64	1.09	7.97
samples	0.4	0.2	1077	1.6	1.05	7.98
	0.7	0.31	821	1.43	1.01	7.90
	1.3	0.63	804	1.34	0.90	7.98

maxima of the very narrow pore size distributions are found at $r_p = 1.6$ nm. The XRD patterns indicate the cubic unit-cell with a dimension of 7.5–8.0 nm.

The deposition of $VO(acac)_2$ on the MCM-48 material reduces the surface area and the porosity, due to the bulky acetylacetonate ligands of the complex. The pore maximum of the pore size distribution shifts drastically to a lower value. After the thermal conversion of the adsorbed complex both the surface area and porosity features are restored to a certain extent, due to the removal of the acetylacetonate ligands. Table 1 summarizes the XRD and BET characteristics of the MCM-48-supported vanadium oxides, obtained after deposition of $VO(acac)_2$ and subsequent thermal conversion. Samples are prepared with increasing vanadium loading (0–1.33 mmol g^{-1} or 0–6.5 wt% V), using the optimized synthesis conditions described earlier (5, 8). The surface areas, pore volumes, pore radii and unit-cell parameters of the supported vanadium samples are compared with the blank MCM-48 support. The change in unit-cell parameter is negligible, which shows that the cubic MCM-48 structure is maintained. The pore radius, pore volume, and surface area shift to lower values as a function of the vanadium loading. This reduction of the porosity in comparison to the blank MCM-48 is due to the narrowing of the pores after the deposition of the vanadium oxide layer.

These XRD and BET characterizations clearly reveal that the deposition of the $VO(acac)_2$ complex and the subsequent thermal conversion results in a supported vanadium oxide catalyst with the characteristic MCM-48 properties.

The interaction between $VO(acac)_2$ and MCM-48. The $VO(acac)_2$ complex can interact with the support surface by a hydrogen bond or a ligand exchange mechanism. An excellent way to determine the actual mechanism of the reaction is the calculation of the ratio R (5–8):

$$R = \frac{\text{mmol (acac) (g support)}^{-1}}{\text{mmol V (g support)}^{-1}} = \frac{n_{acac}}{n_V}.$$

n_{acac} is determined by measuring the weight loss of the modified support in an oxygen flow at 500°C. n_V is determined by colorimetry. If the complex interacts by hydrogen bonding the R value should equal the number of acetylacetonate ligands. A lower value is an indication for the ligand exchange mechanism.

The R values of the $VO(acac)_2$-modified MCM-48 materials equal 1.8, which suggests that the complex reacts both by hydrogen bonding and ligand exchange. This would mean that a part of the acac ligands are evolved and covalently bonded vanadium species are present, besides the hydrogen bonded $VO(acac)_2$. This is a quite interesting observation as the reaction is carried out in the liquid phase at room temperature. The liquid phase deposition of $VO(acac)_2$ on amorphous silica proceeds exclusively by hydrogen bonding (7–9), the corresponding R value is 2. A ligand exchange reaction with silica occurs only during the gas phase modification (7, 8) (sublimation of the complex in vacuum at 120–180°C and subsequent reaction with the substrate; the elevated temperatures increase the reactivity of the complex and the support).

Additional information on the interaction mechanism of $VO(acac)_2$ with MCM-48 is provided by ESR spectroscopy. ESR is a powerful technique for detecting the presence and the coordination geometry of the paramagnetic V^{4+} (d^1) species. The ESR spectra of the $VO(acac)_2$-modified MCM-48 material are typical for V^{4+} in an axial to slightly rhombic environment with the characteristic number of hyperfine lines due to its nuclear spin I of 7/2. The ESR parameters obtained after simulation are summarized in Table 2. It is important to stress that only one well-resolved V^{4+} ESR signal is observed and that there are no indications for the presence of a broad background signal, which could be due to clustered V^{4+}-species. This indicates that

TABLE 2

ESR Parameters of $VO(acac)_2$-Loaded Supports and Some Reference Materials Obtained after Spectrum Simulation

Material	g_{xx}	g_{yy}	g_{zz}	A_{xx} (G)	A_{yy} (G)	A_{zz} (G)	g_{iso}	A_{iso} (G)	Reference
$VO(acac)_2$/MCM-48	1.990	1.988	1.946	74	79	194	1.975	116	This work
$VO(acac)_2/Al_2O_3$	1.984	1.982	1.947	85	90	209	1.971	128	9
$VO(acac)_2/SiO_2$	1.957	1.988	1.948	62	87	202	1.964	117	9
$VO(acac)_2$ in toluene	1.996	1.996	1.944	68	68	191	1.979	109	9
Hydrated V^{4+}/Al_2O_3	1.958	1.988	1.948	72	94	204	1.965	123	28
Hydrated V^{4+}/SiO_2	1.958	1.983	1.947	85	90	209	1.963	128	28

V^{4+} is well-dispersed on the MCM-48 surface after synthesis. In a previous paper, the interaction of the $VO(acac)_2$ complex with the alumina support has been discussed in detail (9) and the spectroscopic results were compared with those obtained for the interaction of the same complex with a silica support. The corresponding ESR parameters of these samples obtained after spectrum simulation, together with some reference materials, are included in Table 2. Due to the higher chemical reactivity of alumina in comparison to silica, a ligand exchange reaction occurs on alumina, resulting in the formation of covalently bonded vanadium species. Table 2 shows that the ESR parameters of the $VO(acac)_2$-modified MCM-48 material are close to those previously obtained for the $VO(acac)_2$-modified Al_2O_3 sample, although this does not means per se that a ligand exchange reaction is taking place. The only difference we noticed with the $VO(acac)_2$-modified Al_2O_3 sample is the broader linewidth because of Al-broadening ($I = 5/2$) due to the close presence of the alumina support. The V^{4+}-species observed at the surface of MCM-48 has a clear vanadyl character [VO^{2+}], which means that one of the vanadium-oxygen bonds is particularly short and can be described in terms of a V=O bond. Thus, V^{4+} experiences a tetragonal compression on the z axis. The average values of g (calculated as $g_{iso} = (g_{xx} + g_{yy} + g_{zz})/3$) and A (calculated as $A_{iso} = (A_{xx} + A_{yy} + A_{zz})/3$) of Table 2 are, according to the empirical correlation diagram of Davidson and Che (13), typical for a 5- and 6-coordinated vanadyl species; i.e., $(VO^{2+})_{5c}$ and $(VO^{2+})_{6c}$, respectively. Both species are difficult to distinguish by ESR because the sixth ligand is only weakly interacting. Thus, the distorted octahedral coordination is one in which an additional ligand is completing the coordination sphere. This axial coordination is expected to be the most pronounced for a V^{4+} species with g and A values close to axial symmetry. This is indeed the case for the ESR parameters of the $VO(acac)_2$-modified MCM-48 material. Thus, a distorted square pyramidal coordination is the most likely coordination model for V^{4+} on MCM-48.

The ESR measurements reinforce our conclusion that the MCM-48 surface exhibits higher reactivity in comparison to the amorphous silica support. The surface of silica terminates in either a siloxane group (≡Si–O–Si≡) with oxygen on the surface or one of several forms of silanol groups (≡Si–OH; free, bridged and/or geminal silanols). The calcination procedure of the as-synthesized MCM-48 precursor, which is carried out to remove the gemini surfactant molecules, leaves the substrate covered only with siloxane bridges and isolated hydroxyl groups (6). It has been reported that the OH groups on the surface of MCM-48 exhibit only weak acidity, comparable with the OH groups on silica (14). This can also be inferred from Figs. 1a and 1e, which present the infrared spectra of the pure MCM-48

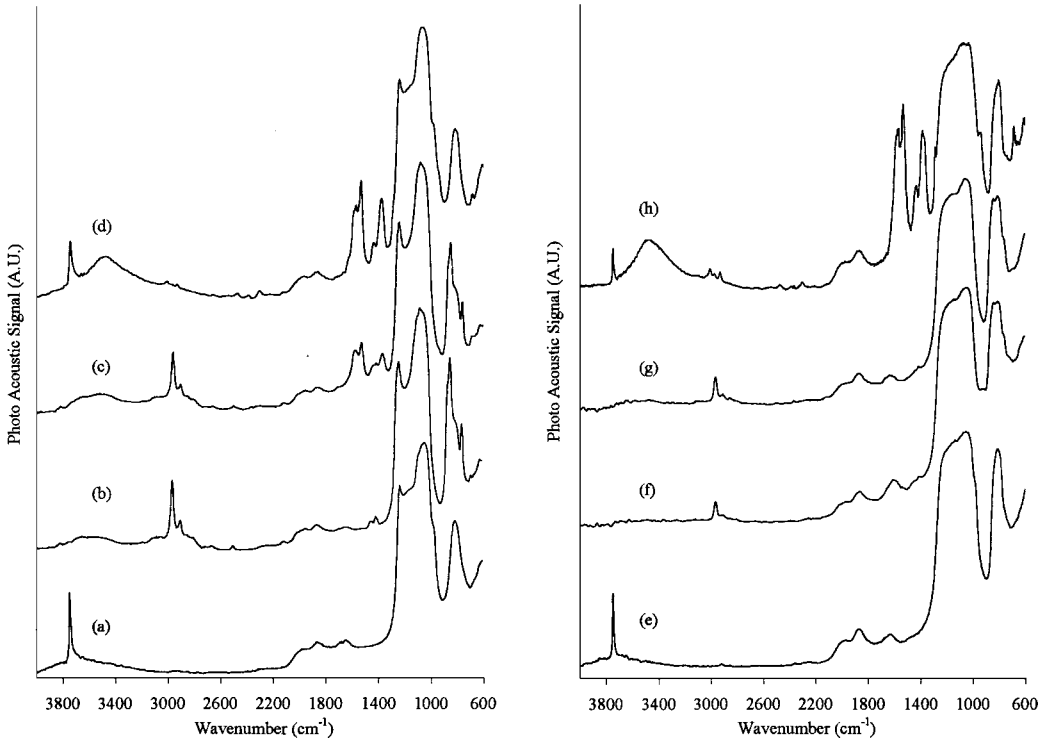

FIG. 1. FTIR-PA spectra of (a) pure MCM-48 after pretreatment at 550°C, (b) MCM-48 modified with HMDS, (c) MCM-48 after modification with HMDS and $VO(acac)_2$, (d) MCM-48 after modification with $VO(acac)_2$, without HMDS pretreatment, (e) pure silica support after pretreatment at 700°C, (f) silica modified with HMDS, (g) silica after modification with HMDS and $VO(acac)_2$, (h) silica after modification with $VO(acac)_2$, without HMDS pretreatment.

support after pretreatment at 550°C, and of the pure silica support pretreated at 700°C, respectively. Pretreatment of the silica support at 700°C results in dehydration and dehydroxylation reactions, leaving the silica surface also covered only with isolated silanols and siloxane bridges. The spectra in Figs. 1a and 1e exhibit a band at 3747 cm^{-1}, attributed to the isolated OH. A differing acid–base character between the OH groups on silica and MCM-48 would result in a different position of this characteristic band.

In order to study the surface properties of the MCM-48 material and to compare the interaction mechanism of the $VO(acac)_2$ complex with MCM-48 and silica respectively, an additional set of experiments was performed. First, the silanolgroups on both supports (after pretreatment at 550 and 700°C for MCM-48 and silica, respectively) were deactivated prior to the reaction with $VO(acac)_2$, in order to study the influence on the deposition of the complex. A typical chemical modification technique is the reaction of the silica surface with hexamethyldisilazane (HMDS) (15). This reaction is known as a trimethylsilylating, deactivating reagent in chromatography, but is also very useful for the quantification of the silanol number. HMDS reacts readily with the silanols, yielding very stable trimethylsilyl groups according to the following reaction (15):

$$2 \equiv \text{Si-OH} + (CH_3)_3\text{-Si-NH-Si-}(CH_3)_3 \rightarrow 2 \equiv \text{Si-O-Si}(CH_3)_3 + NH_3.$$

No side reactions have been detected. The NH_3 is evolved during the reaction at room temperature. The on-line determination of the liberated NH_3 directly yields the number of silanols reacted with HMDS. However, after modification of the silica surface with HMDS all the hydroxyls are converted into trimethylsilyl groups. This is also shown in Fig. 1. Figures 1b and 1f present the infrared spectra of respectively the MCM-48 and the silica support after reaction with HMDS. The band at 3747 cm^{-1} has disappeared, whereas in the region around 2950 cm^{-1} the methyl bands are present. If these pretreated samples are subsequently modified in a liquid phase reaction with $VO(acac)_2$ it can be inferred if the complex reacts selectively with the OH groups of the support. A similar study on the treatment of amorphous silica with HMDS followed by treatment with $Cr(acac)_3$ has been analyzed by Haukka *et al.* (16). The $VO(acac)_2$, modified samples are presented in Figs. 1c and 1g, respectively. In spectrum 1c the IR bands between 1200 and 1600 cm^{-1} are attributed to the acetylacetonate ligands of the adsorbed complex. The vanadium determination reveals a loading of 0.12 mmol g^{-1} (0.6 wt% V) and the corresponding *R* value is 2. The vanadium loading of the modified MCM-48 support using the same reaction conditions, without the HMDS pretreatment is 0.4 mmol g^{-1} (2 wt% V). In Fig. 1g the spectrum of the HMDS pretreated silica support is shown after modification with $VO(acac)_2$ under the same reaction conditions. No acac bands are observed in the IR and the chemical analysis traced only a negligible amount of vanadium. In comparison, the infrared spectra of the $VO(acac)_2$-modified MCM-48 and silica supports, without the HMDS pretreatment, are shown in Figs. 1d and 1h, respectively. The broad band between 3600 and 3200 cm^{-1} is assigned to hydrogen bonded silanol groups, indicating the presence of hydrogen bonded $VO(acac)_2$.

It can be inferred that the $VO(acac)_2$ reacts selectively with the OH groups of the support, but on MCM-48 there are also other surface sites, in particular the siloxane groups, contributing to the adsorption process of the complex. It was already established earlier (16) that on silica the concentration of the siloxane bridges increases with rising pretreatment temperatures, as the remaining free silanol groups dehydroxylate. Simultaneously, the reactivity enhances, as structural changes occur, giving rise to the so-called *strained* siloxane bridges. This site is assumed to be an unsymmetrical siloxane bridge consisting of one silicon atom being more electron deficient than the other. The MCM-48 support is only covered with 0.9 OH/nm^2 (6, 17, 18). A part of the siloxane bridges are probably strained groups, resulting in a much higher reactivity in comparison to amorphous silica, and the $VO(acac)_2$ can interact with this surface site too.

It is particularly interesting to elucidate the nature of the interaction of the $VO(acac)_2$ complex with the strained Si–O–Si sites, as this provides valuable information on the surface properties of the MCM-48. The ESR study suggested an alumina-like behavior of MCM-48. On alumina, a ligand exchange reaction results in the formation of a covalently bonded vanadyl species. The acac ligand(s) evolved during this reaction, subsequently react with coordinatively unsaturated Al^{3+} species to Al-acac species (which gives *R* values of 2 for this reaction as, in fact, no acac is evolved (9)). A ligand exchange mechanism with the strained Si–O–Si groups on MCM-48 would result in the formation of a covalently bonded Si–O–VO(acac) species and simultaneously the formation of Si(acac) (in analogy to alumina (9)). However, it is generally known that Si(acac) compounds are extremely unstable. In fact, no values are reported for the mean metal–oxygen bond dissociation enthalpy, as these compounds are too unstable to be studied (the highest metal–oxygen bond dissociation enthalpies are (19): $Al(acac)_3$, 242 kJ/mol; and $Be(acac)_2$, 274 kJ/mol). Therefore, a formation of Si(acac) species is very unlikely.

Moreover, the *R* value of the reaction of $VO(acac)_2$ with the pure (non-HMDS-pretreated) MCM-48 is 1.8, suggesting the release of acac ligands. However, the reaction of the complex with the HMDS pretreated support is 2. The explanation for this difference was revealed by studying the effect of water on the formation of the various surface species. When the HMDS pretreated MCM-48 was modified with $VO(acac)_2$ under "wet" conditions, the *R* value of

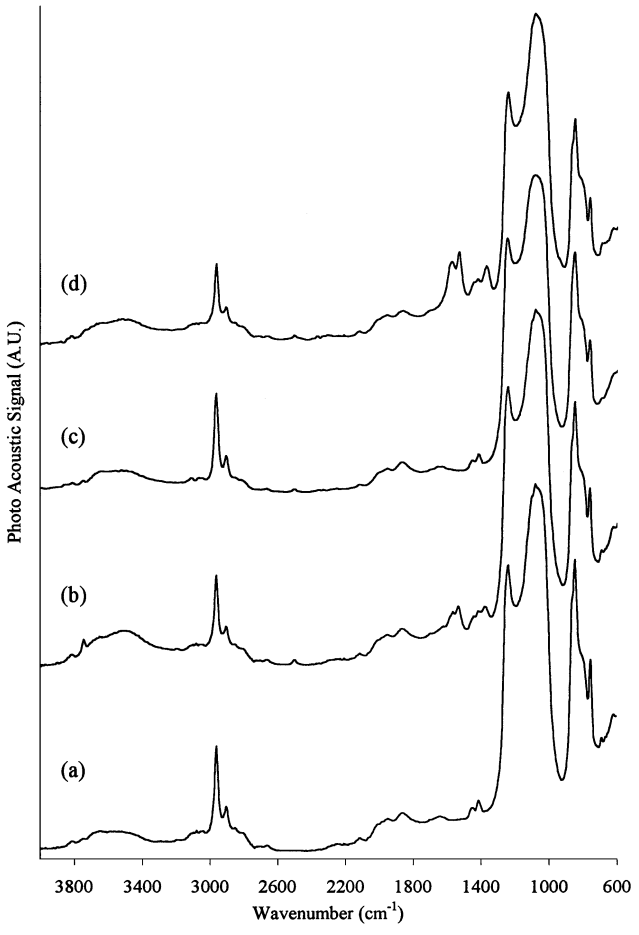

FIG. 2. FTIR-PA spectra of (a) MCM-48 modified with HMDS, (b) HMDS-pretreated MCM-48 after reaction with $VO(acac)_2$ under "wet" conditions, (c) HMDS-pretreated MCM-48 stirred in "wet" toluene in the absence of $VO(acac)_2$, (d) MCM-48 after modification with HMDS and $VO(acac)_2$ (dry conditions).

the reaction was 1.1. The wet conditions refer to the fact that the complex and the solvent used for the liquid phase modification were not dried prior to the reaction (for all other experiments the reagents are dried before reaction). Furthermore, the IR spectra of the sample prepared under wet conditions (Fig. 2b), still exhibits the characteristic acac bands, but it is obvious that some OH groups are generated as well. A control experiment to elucidate the formation of these Si–OH groups is carried out by stirring the HMDS pretreated sample in "wet" toluene, in the absence of $VO(acac)_2$. The IR spectrum of this control experiment in Fig. 2c shows no significant generation of Si–OH groups. The hydrophobic trimethylsilyl groups prevent the surface from direct rehydroxylation. Indeed, the rather low stability of MCM-48 toward moisture can be improved drastically by trimethylsilylation (20). Apparently, even with the hydrophobic nature of the sample, water can still interact with the surface sites involving vanadium species. It is anticipated that the presence of traces of H_2O will result in a conversion of the strained siloxane–$VO(acac)_2$ system, with the formation of a covalently bonded vanadium species and the simultaneous generation of Si–OH species and release of acetylacetone (Hacac). Similarly, the $VO(acac)_2$ modified MCM-48 sample (without HMDS pretreatment) is sensitive to exposure to air or traces of water, which results in the immediate conversion of the surface species involving a strained siloxane–$VO(acac)_2$ system. This explains the lower *R* values for non-HMDS-pretreated MCM-48, as the HMDS-pretreated samples are stabilized by the trimethylsilyl groups. The hydrophobic nature prevents the uptake of water before characterization. However, the presence of water during the modification of the HMDS pretreated MCM-48 with $VO(acac)_2$, also results in lower *R* values, due to the *in situ* conversion of the strained siloxane–$VO(acac)_2$ system.

In conclusion, the analytical (*R* value), spectroscopic (ESR), and chemical (selective site blocking by HMDS pretreatment) results evidence that the MCM-48 surface exhibits much higher reactivity in comparison to amorphous silica. The reaction of MCM-48 with $VO(acac)_2$ yields two types of adsorbed complexes. The $VO(acac)_2$ can interact by hydrogen bonding with the surface silanols. In addition, a part of the complexes can interact with the very reactive strained siloxane groups of the MCM-48 as well. This results in the formation of a strained siloxane–$VO(acac)_2$ system, which is envisaged in Scheme 1. Exposure to air (water) converts this system, with formation of a covalently bonded species and generation of Si–OH groups (Scheme 1).

The difference in reactivity between the MCM-48 and the silica surface can be explained by the number of strained

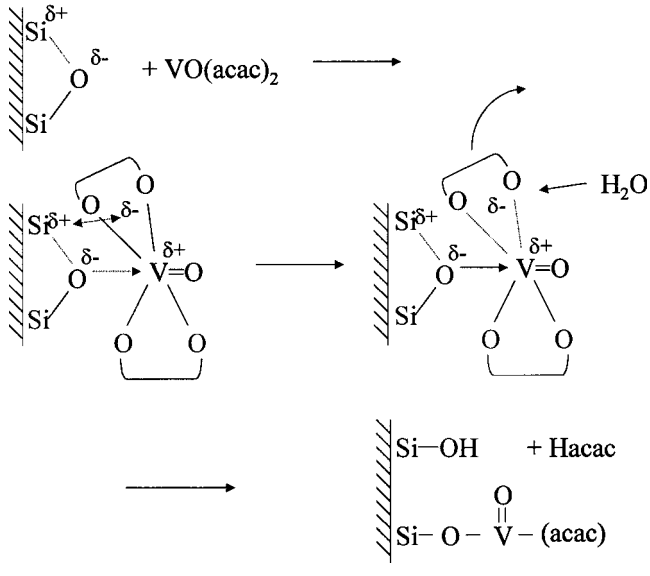

SCHEME 1. Schematic presentation of the reaction mechanism of the adsorption of $VO(acac)_2$ on MCM-48.

TABLE 3

Comparison between the Spectral Features and the Inferred Supported VO_x Structure for MCM-48 and Silica-Supported Vanadium Oxides, Respectively

V loading			Spectral features of supported vanadium oxide							
	V/nm^2		Raman (cm^{-1})		FTIR (cm^{-1})		UV-DR (nm)		VO_x structure	
mmol/g	MCM	Silica	MCM	Silica	MCM	Silica	MCM	Silica	MCM	Silica
0.2	0.10	0.40	1039	1042	930	930	250, 301	250, 301, 350	T_d, mono	T_d, mono/chains
0.4	0.20	0.94	1039	1042	930	926	250, 301	250, 301, 350	T_d, mono	T_d, mono/chains
0.7	0.31	1.39	1039	1042, 993	923	924	250, 301, 354	250, 301, 350, 440	T_d, mono/chains	T_d, mono/chains + O_h
1.3	0.63	1.75	1039, 993	1042, 993	920	924	250, 301, 354, 425	250, 301, 350, 440	T_d, mono/chains + O_h	T_d, mono/chains + O_h

siloxane groups and the difference in surface area. In the case of MCM-48, there are more strained groups, and the surface area is approximately four times higher than the surface area of silica. Accordingly, the reactivity per gram is much higher for MCM-48.

Spectroscopic Study of the MCM-48-Supported Vanadium Oxide

The thermal conversion of the supported $VO(acac)_2$ complex occurred at around 300°C as evidenced by the disappearance of the V^{4+} ESR signal upon calcination. After calcination the supported vanadium oxide species formed can be present in several VO_x configurations. From the monomeric and dimeric tetrahedral structure, the one- and two-dimensional chains of tetrahedral species to more polymeric species and even crystals of vanadium pentoxide. Several spectroscopic techniques are used to study the structure of the deposited VO_x phase on the MCM-48 surface, and the results are summarized in Table 3.

Raman spectroscopy. The Raman spectra of the MCM-48-supported VO_x catalysts show characteristic bands of the MCM-48 support material (21, 22) at 430, 498, and 800 cm^{-1}. In Fig. 3 the Raman spectra are presented as a function of the vanadium loading. The strong band at 1039 cm^{-1} is characteristic for the stretching vibration of terminal V=O bonds in monomeric, tetrahedral vanadia surface species with three bonds to the support surface ($(SiO)_3V{=}O$) (21, 23). Spectrum 2d clearly exhibits a strong band at 993 cm^{-1} which is attributed to crystalline V_2O_5 (21, 23) (other characteristic bands of V_2O_5 are present at 703, 407, 285, and 146 cm^{-1}). However, XRD measurements showed no evidence for the formation of a crystalline fraction of vanadium oxide. This suggests that at this loading (1.33 mmol g^{-1}), an aggregation of the vanadium centers results in the formation of microcrystallites of V_2O_5. Traces of these species can easily be detected by Raman spectroscopy, but are not observed by XRD.

It has been reported earlier that silica supported vanadium oxides exhibit Raman features of crystalline V_2O_5 at loadings >0.6 mmol g^{-1} (24). Obviously, the higher surface area of the MCM-48 support in comparison to silica enables the deposition of higher vanadium loadings before a crystalline fraction of vanadium oxide appears. However, when comparing the actual number of vanadium sites per nm^2 on MCM-48 and silica (Table 3), it is remarkable that part

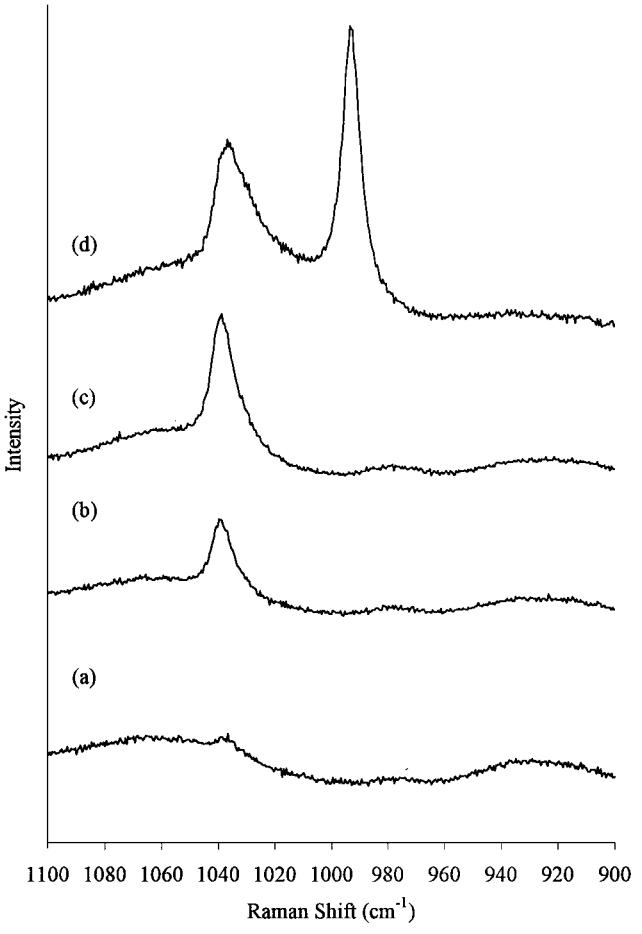

FIG. 3. Raman spectra of MCM-48 supported vanadium oxide catalysts with respective vanadium loading of 0.2 mmol/g (a), 0.4 mmol/g (b), 0.7 mmol/g (c), and 1.3 mmol/g (d).

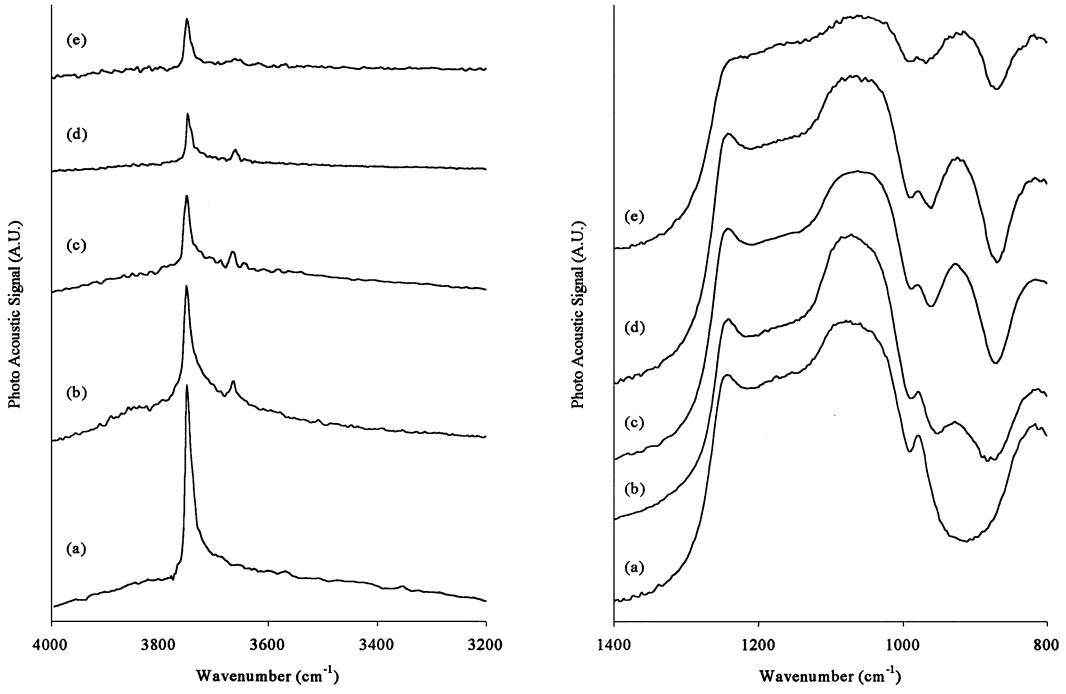

FIG. 4. FTIR-PA spectra of pure MCM-48 (a) and MCM-48-supported vanadium oxides with respective vanadium loading of 0.2 mmol/g (b), 0.4 mmol/g (c), 0.6 mmol/g (d), and 1.3 mmol/g (e).

of the MCM-48 surface still remains uncovered, although crystalline V_2O_5 appears (sample with coverage 0.63 in Table 3). When a certain vanadium loading is reached, the grafted VO_x groups clearly tend to the formation of clusters on the support surface, leaving parts of the support surface uncovered.

FTIR spectroscopy. In Fig. 4 the infrared spectra are shown of the MCM-48 supported vanadium oxides as a function of the vanadium loading. The intensity of the free silanol band at 3745 cm^{-1} decreases with an increasing amount of deposited vanadium, owing to the formation of Si–O–V bonds. The silanols are gradually consumed upon higher vanadium loadings, except for the sample with the highest loading (1.33 mmol/g, Fig. 4e).

The band at 3660 cm^{-1} is attributed to the presence of V–OH surface species (24). Apparently, this band shows no evolution as a function of the vanadium loading. These V–OH species most likely generate from the reaction of the deposited vanadium oxide structures with ambient water, and are not due to structural rearrangements at higher loadings.

The IR bands at 1248, 1080, and 978 cm^{-1} are attributed to the framework of the MCM-48 material (25). The presence of these bands in the supported vanadium oxide samples confirms that the structural MCM-48 properties are maintained. These bands are not observed in amorphous silica. The intensity of a band at 930 cm^{-1} increases with increasing vanadium loading. With loadings above 0.7 mmol g^{-1} (Figs. 4d and 4e), a slight shift towards lower wavenumbers (923 cm^{-1} in Fig. 4d and 920 cm^{-1} in Fig. 4e) is observed. This band is assigned to a Si–O–V stretch (22, 24, 25), although the literature assignments also mention a contribution of both Si–O–V and V–O–V bridges (25). However, the characteristic IR bands of V–O–V in crystalline V_2O_5 are generally observed at around 830–850 cm^{-1} (26, 27). The shift to lower wavenumbers probably indicates that at low vanadium loadings only Si–O–V (in an isolated tetrahedral $(Si–O)_3V{=}O$ configuration) occurs, whereas with increasing loading V–O–V linkages start to appear.

At a loading of 1.33 mmol g^{-1} the aggregation of vanadium centers results in the formation of crystalline V_2O_5, which gives rise to a surface with both covered and uncovered patches of MCM-48. This explains why the intensity of the OH band in Fig. 4e does not decrease significantly in comparison to Fig. 4d.

Similar conclusions for the change in the Si–OH and Si–O–V regions are drawn from the IR study of silica supported vanadium oxides (Table 3).

UV–vis diffuse reflectance spectroscopy. UV–vis diffuse reflectance spectroscopy is a very useful technique to infer information on the coordination of vanadium. The energy of the oxygen → vanadium charge transfer bands (CT bands) is dependent on the number of oxygen atoms surrounding the central V^{5+}. A lower coordination number generally results in a shift of the charge transfer transition to higher energy (lower wavelength) (5, 8, 21, 23, 28).

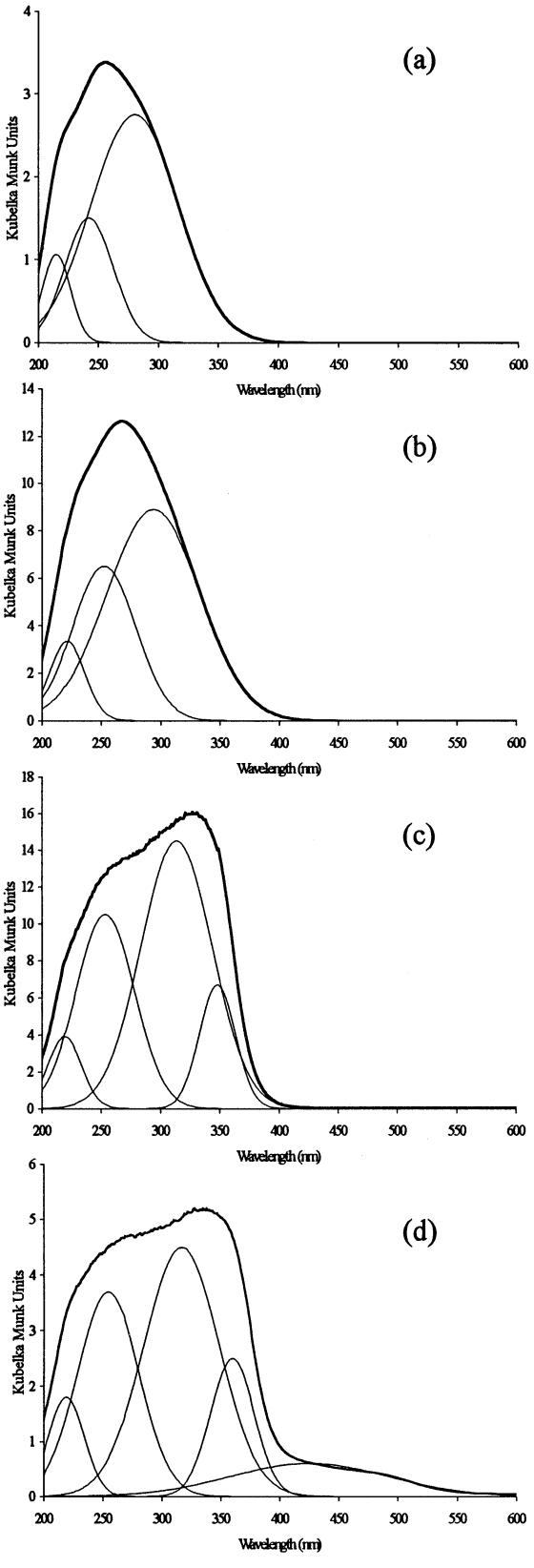

FIG. 5. Deconvoluted UV–vis diffuse reflectance spectra of MCM-48-supported vanadium oxide catalysts with respective vanadium loading of 0.2 mmol/g (a), 0.4 mmol/g (b), 0.7 mmol/g (c), and 1.3 mmol/g (d).

The UV–vis-DR spectra of MCM-48 supported VO_x are shown in Fig. 5. The spectra have been deconvoluted to distinguish between different surface VO_x species. A clear evolution as a function of the vanadium loading is observed.

Apparently, there are 5 different charge transfer bands, around 219, 250, 301, 354, and 425 nm, respectively. Up to a vanadium loading of 0.7 mmol g^{-1} (Figs. 5a to 5c) the samples show exclusive bands in the 200- to 400-nm region. The band at 219 nm is attributed to the MCM-48 support. The area of the bands at 250 and 301 nm increases almost linearly as a function of the vanadium loading. These bands are assigned to isolated tetrahedral VO_x (29) on the surface of the MCM-48, as evidenced by the 1039 cm^{-1} Raman shift in Fig. 3 and the infrared study in Fig. 4. At a loading of 0.7 mmol g^{-1} a surface species appears related to a CT band at 354 nm. We attribute this band to the presence of tetrahedral chains of VO_x, linked to each other by V–O–V bridges. This can be explained by the condensation of the monomeric species to form chain-like clusters with the vanadium centra in a tetrahedral configuration. The sample with the highest loading (1.33 mmol g^{-1}, Fig. 5d) shows an additional absorption above 400 nm, indicating the presence of polymeric chains and even small crystallites of V_2O_5. At this loading the MCM-48 surface is heterogeneously covered with monomers, chains, and microcrystallites of vanadium oxide.

The observed charge transfer bands in the case of the silica-supported vanadium oxide, are summarized in Table 3 (spectra are not presented). The much lower surface area on silica results in the formation of chain-like species (CT band at around 350 nm) at much lower vanadium loading (already at 0.2 mmol g^{-1}) then that seen in the MCM-48 samples. Also a large fraction of octahedral species occurs at lower loading on silica.

From the spectroscopic comparison of the grafted vanadium oxide on MCM-48 and amorphous silica it can be concluded that the enormous gain in surface area when using the MCM-48 support is certainly an advantage in the preparation of highly dispersed supported vanadium oxides. Higher vanadium loadings can be obtained before octahedral or crystalline vanadium oxide appears.

Oxidation of Methanol

Supported vanadium oxides possess unique properties in several heterogeneous catalytic processes, e.g., the oxidation of sulfur dioxide to sulfur trioxide (30) in the preparation of sulfuric acid, the oxidation of *o*-xylene to phthalic anhydride (31, 32), and the selective catalytic reduction of NO_x (30, 33). The oxidation of methanol is an important probe reaction to study the catalytic properties of surface vanadium oxide species (7, 30, 32, 34, 35). The product selectivity reflects the reaction pathways that depend on the acidic, basic, or redox sites on the catalyst

TABLE 4

Oxidation of Methanol at 400°C

V (mmol/g)	V/nm^2	VO_x structure	Conversion (%)	Selectivity (%)			Yield (%)		
				$CO+CO_2$	HCHO	CH_3OCH_3	$CO+CO_2$	HCHO	CH_3OCH_3
VO_x/MCM-48									
0.0	0.00	—	15.3	0.0	2.7	97.3	0.0	0.4	14.9
0.2	0.10	T_d, mono	31.0	0.0	98.1	1.9	0.0	30.4	0.6
0.4	0.20	T_d, mono	60.9	3.4	94.7	1.9	2.1	57.7	1.2
0.7	0.31	T_d, mono/chains	75.0	5.0	92.8	2.2	3.8	69.6	1.7
1.3	0.63	T_d, mono/chains + O_h	68.1	46.8	33.9	19.3	31.9	23.1	13.1
VO_x/silica									
0.0	0.00	—	9	0.0	11.1	88.9	0.0	1.3	10.7
0.2	0.40	T_d, mono/chains	21.0	0.0	79.3	20.7	0.0	16.6	4.4
0.4	0.94	T_d, mono/chains	45.0	8.0	88.0	4.0	3.6	39.6	1.8
0.7	1.39	T_d, mono/chains + O_h	58.0	20.3	72.5	7.2	11.8	42.0	4.2
1.3	1.75	T_d, mono/chains + O_h	31.0	41.2	38.5	20.3	12.7	12.1	6.2

Note. Catalytic performance (conversion, selectivity, and yield) of the MCM-48 and silica-supported vanadium oxides as a function of the vanadium loading.

surface. Acidic sites give rise to dimethyl ether, basic sites produce carbon oxides (CO_x) and redox sites produce formaldehyde, methyl formiate, and dimethoxymethane. Silica-supported vanadium oxides show a rather low activity for the oxidation of methanol, in comparison to other frequently used oxide supports like alumina and titania (28, 32). However, VO_x/SiO_2 catalysts are very selective toward formaldehyde.

In this study the influence of the vanadium loading on the catalytic properties has been studied for the oxidation of methanol and the results are shown in Table 4. The conversion, selectivity, and yield are presented as a function of the vanadium loading. The reaction was carried out at 400°C at atmospheric pressure. The pure MCM-48 exhibits rather low activity (15% conversion at 400°C). However, the conversion level is significantly higher than that amorphous silica (9% conversion at 400°C). The reaction of methanol on the MCM-48 surface yields dimethylether, which suggests the presence of acidic sites. This is an additional indication that the surface of MCM-48 contains sites with higher reactivity in comparison with silica. This was attributed to the presence of strained siloxanes, which indeed can act as Lewis acid center (15).

The conversion level increases with increasing loading of vanadium. The major product is formaldehyde, produced at the $(SiO)_3V{=}O$ redox sites. The spectroscopic study evidenced that with higher vanadia coverage (on MCM-48, the sample with 0.7 mmol g^{-1} V) polymeric chains with V–O–V bridges appear. However, the conversion and selectivity level still increases, which means that these V–O–V bridges do not affect the reaction. It has already been reported (30, 34, 36) that the active sites on supported vanadium oxide catalysts for the oxidation of hydrocarbons, are rather the V–O–support bonds than the terminal V=O or bridging V–O–V. Therefore, the catalytic properties of the vanadium oxide layer can be altered by varying the oxide support. Titania and alumina for example give rise to much stronger V–O–support bonds and simultaneously the activity for the methanol oxidation enhances too.

The samples containing a fraction of crystalline vanadium oxide (indicated as O_h in Table 4) show a decreased activity (only a slight effect on the MCM-48 sample), as the vanadium sites in the crystal lattice of V_2O_5 are less or not accessible. In addition, the formaldehyde yield is drastically reduced, and carbon oxides (CO and CO_2) are formed. The increased conversion to dimethylether (on acidic sites) is due to the aggregation of V_2O_5 crystals, leaving a part of the support surface uncovered. Vanadium oxide itself only shows a weak acidic character (36).

Basically, on both MCM-48 and silica, the VO_x centers are linked to the surface via Si–O–V bonds. However, the supported VO_x/MCM-48 catalysts exhibit a better catalytic performance. Especially higher yields of formaldehyde can be obtained on the supported MCM-48 catalysts in comparison to the silica samples with the same vanadium loading (Table 4). This confirms the spectroscopic results, evidencing that the higher surface area of MCM-48 enables the deposition of a higher loading of vanadium, with the VO_x still in a very well dispersed and catalytically active tetrahedral coordination.

In order to determine if the properties of the MCM-48 material are maintained after a catalytic run of 24 h time on stream, XRD and BET measurements of the VO_x/MCM-48 catalysts are performed. Figure 6 shows the XRD patterns and pore size distributions of a sample before and after the reaction. This reveals that the characteristic crystallinity and porosity features have not changed significantly. The intensity of the XRD reflections is slightly reduced, but the

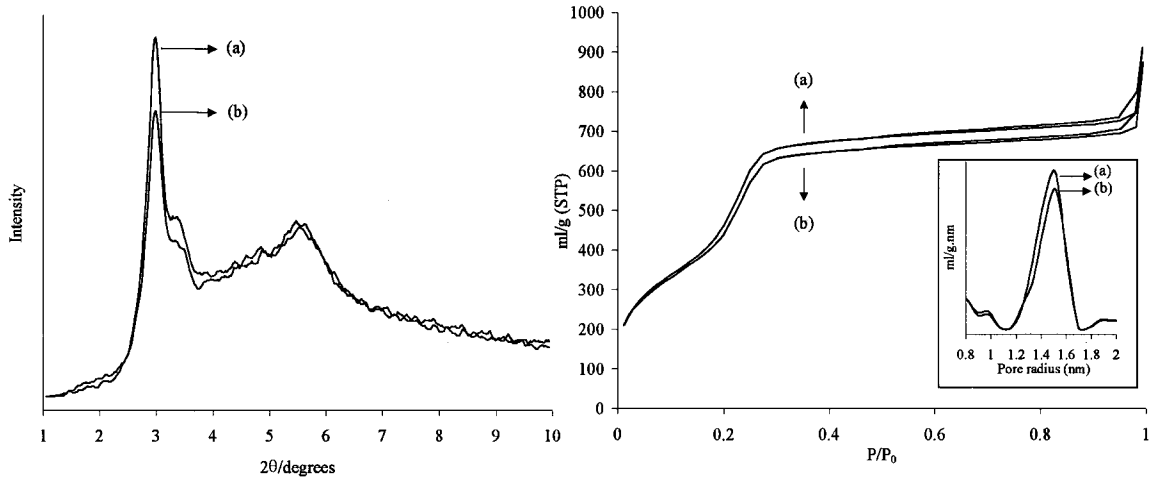

FIG. 6. XRD patterns (left) and nitrogen sorption isotherms (inset, pore size distributions) (right) of MCM-48-supported vanadium oxide sample before (a) and after (b) catalytic run of 24 h.

unit-cell parameter does not change. The pore size distribution still shows mesoporosity and the surface area, pore volume and pore radius are nearly the same as before the catalytic reaction.

CONCLUSIONS

The preparation of MCM-48 supported vanadium oxide catalysts by means of the molecular designed dispersion of $VO(acac)_2$ has been investigated and compared with the preparation of silica supported VO_x. The analytical, spectroscopic, and chemical results evidence that the MCM-48 exhibits strained siloxane groups which are much more reactive in comparison to the siloxane groups on amorphous silica. Therefore the reaction of $VO(acac)_2$ with the MCM-48 surface yields two types of adsorbed $VO(acac)_2$ species. Hydrogen bonding occurs between the OH groups of the support and the acac ligands of the complex. In addition, the complex also interacts with the highly reactive strained siloxanes of MCM-48.

Porosity, X-ray diffraction and infrared data show that the MCM-48 properties are maintained after grafting with VO_x species. Spectroscopic characterization of the supported VO_x/MCM-48 by FTIR, Raman, and UV–vis–DR spectroscopy shows the presence of different VO_x structures as a function of the surface loading. At loadings up to 0.7 mmol g^{-1} (3.5 wt% V) the MCM-48 surface is uniformly covered with tetrahedral $(SiO)_3V{=}O$ monomers. With increasing loadings, polymer chains of tetrahedral VO_x appear, which are linked to each other with V–O–V bridges. At surface loadings of 1.33 mmol g^{-1} (6.7 wt% V) also a small fraction of crystalline V_2O_5 is formed. Nevertheless, due to the high surface area of the MCM-48 support, higher vanadium loadings can be obtained in comparison to an amorphous silica support before crystalline vanadium oxide appears.

The oxidation of methanol as probe reaction reveals the reactivity and stability of the VO_x/MCM-48 catalysts. In addition, the high surface area and the narrow pore size distribution of this catalyst system provides great potential use in various reactions.

ACKNOWLEDGMENTS

This work was supported by the F.W.O. Vlaanderen (Research Project G.0446.99). M. Baltes thanks the F.W.O. Vlaanderen for a research grant. P. Van Der Voort and B. M. Weckhuysen are postdoctoral fellows of the F.W.O. Vlaanderen.

REFERENCES

1. Kresge, C. T., Leonowicz, M. E., Roth, W. J., Vartuli, J. C., and Beck, J. S., *Nature* **359**, 710 (1992).
2. Kresge, C. T., Leonowicz, M. E., Roth, W. J., and Vartuli, J. C., U.S. patent 5098684.
3. Huo, Q., Margolese, D. E., and Stucky, G. D., *Chem. Mater.* **8**, 1147 (1996).
4. Van Der Voort, P., Mathieu, M., Mees, F., and Vansant, E. F., *J. Phys. Chem.* **102**, 8847 (1998).
5. Van Der Voort, P., Babitch, I. B., Grobet, P. J., Verberckmoes, A. A., and Vansant, E. F., *J. Chem. Soc. Faraday Trans.* **92**, 3635 (1996).
6. Van Der Voort, P., Morey, M., Stucky, G. D., Mathieu, M., and Vansant, E. F., *J. Phys. Chem.* **102**, 585 (1998).
7. Baltes, M., Van Der Voort, P., Collart, O., and Vansant, E. F., *J. Porous Mater.* **5**, 357 (1998).
8. Baltes, M., Collart, O., Van Der Voort, P., and Vansant, E. F., *Langmuir* **15**, 5841 (1999).
9. Baltes, M., Van Der Voort, P., Weckhuysen, B. M., Rao, R. R., Schoonheydt, R. A., and Vansant, E. F., *Phys. Chem. Chem. Phys.* **2**, 2673 (2000).
10. Weckhuysen, B. M., Rao, R. R., Pelgrims, J., Schoonheydt, R. A., Bodart, P., Debras, G., Collart, O., Van Der Voort, P., and Vansant, E. F., *Chem. Eur. J.* **6**, 2 (2000).
11. Vogel, A. I., "Quantitative Inorganic Analysis," 3rd ed. Longmans, London, 1971.
12. Evans, R., Marconi, U. M. B., and Tarazona, P., *J. Chem. Soc. Faraday Trans. II* **82**, 1763 (1986).

13. Davidson, A., and Che, M., *J. Phys. Chem*. **96**, 9909 (1992).
14. Jentys, A., Pham, N. H., and Vinek, H., *J. Chem. Soc., Faraday Trans.* **92**, 3287 (1996).
15. Vansant, E. F., Van Der Voort, P., and Vrancken, K. C., "Characterization and Chemical Modification of the Silica Surface," Studies in Surface Science and Catalysis. Elsevier, Amsterdam, 1995.
16. Haukka, S., and Root, A., *J. Phys. Chem*. **98**, 1695 (1994).
17. Van Der Voort, P., Mathieu, M., Vansant, E. F., Rao, S. N. R., and White, M. G., *J. Porous Mat.* **5**, 305 (1998).
18. Benjelloun, M., Van Der Voort, P., Cool, P., Collart, O., and Vansant, E. F., *Phys. Chem. Chem. Phys.*, submitted for publication.
19. Ribeiro da Silva, M. A. V., "Metal–Ligand Bond Energies in Coordination Compounds" Proceedings, 11th Summer School on Coordination Chemistry and Catalysis. (J. J. Ziolkowski, Ed.), Karpacz, Poland, 1987.
20. Koyano, K. A., Tatsumi, T., Tanaka, Y., and Nakata, S., *J. Phys. Chem. B* **101**, 9436 (1997).
21. Schraml-Marth, M., Wokaun, A., Pohl, M., and Krauss, H. L., *J. Chem. Soc. Faraday Trans.* **87**, 2635 (1991).
22. Chao, K. J., Whu, C. N., Chang, H., Lee, L. J., and Hu, S., *J. Phys. Chem. B* **101**, 6341 (1997).
23. Scharf, U., Schraml-Marth, M., Wokaun, A., and Baiker, A., *J. Chem. Soc. Faraday Trans.* **87**, 3299 (1991).
24. Van Der Voort, P., White, M. G., Mitchell, M. B., Verberckmoes, A. A., and Vansant, E. F., *Spectrochim. Acta, Part A* **53**, 2181 (1997).
25. Morey, M., Davidson, A., and Stucky, G. D., *J. Porous Mater.* **5**, 195 (1998).
26. Frederickson, L. D., and Hausen, D. M., *Anal. Chem*. **35**, 819 (1963).
27. Reddy, B. M., Ganesh, I., and Chowdry, B., *Catal. Today* **49**, 115 (1999).
28. Catana, G., Rao, R. R., Weckhuysen, B. M., Van Der Voort, P., Vansant, E. F., and Schoonheydt, R. A., *J. Phys. Chem. B* **102**, 8005 (1998).
29. Gao, X., Bare, S. R., Weckhuysen, B. M., and Wachs, I. E., *J. Phys. Chem. B* **102**, 10842 (1998).
30. Deo, G., Wachs, I. E., and Haber, J., *Crit. Rev. Surf. Chem*. **4**, 141 (1994).
31. Dias, C. R., Portela, M. F., and Bond, G. C., *J. Catal.* **157**, 344 (1995).
32. Bond, G. C., and Tahir, S. F., *Appl. Catal.* **71**, 1 (1991).
33. Vogt, E. T. V., Boot, A., van Dillen, A. J., Geus, J. W., Janssen, F. J. J. G., and van den Kerkhof, F. M. G., *J. Catal.* **114**, 313 (1988).
34. Deo, G., and Wachs, I. E., *J. Catal.* **146**, 323 (1994).
35. Van Der Voort, P., Baltes, M., White, M. G., and Vansant, E. F., *Interf. Sci.* **5**, 209 (1997).
36. Wachs, I. E., and Weckhuysen, B. M., *Appl. Catal. A* **157**, 67 (1997).